buildings

MDPI

Article

The Impact of New Composite Curing Agents on the Curing Properties of Glacial Debris in the Pulang Copper Deposit

Qingtian Zeng [1], Xinglong Feng [1], Hanmeng Ren [2], Sugang Sui [3], Shaoyong Wang [2], Wei Sun [4] and Juanhong Liu [2,*]

[1] Yunnan Diqing Non-Ferrous Metal Co., Ltd., Shangri-La City 674400, China; rancher005252@163.com (Q.Z.); mm2196799092@163.com (X.F.)
[2] School of Civil and Resources Engineering, University of Science and Technology Beijing, Beijing 100083, China; 18810289307@163.com (H.R.); wshy0226@163.com (S.W.)
[3] Kunming Prospecting Design Institute of China Nonferrous Metals Industry Co., Ltd., Kunming 650051, China; suisugang2@zskk1953.com
[4] Faculty of Land Resources Engineering, Kunming University of Science and Technology, Kunming 650500, China; kmustsw@kust.edu.cn
* Correspondence: juanhong1966@hotmail.com

Abstract: In recent years, Pulang Copper Deposit has experienced multiple occurrences of debris flow, of varying magnitudes, which have significantly impacted the safety of mining operations. Debris flow has become a major safety hazard of natural caving mining in Pulang Copper Deposit. To address the issues of the formation of debris flow due to the collapse of glacial debris in the Pulang Copper Deposit, this paper proposes new composite curing agents for grouting and curing glacial debris. The study investigates the influence of curing agents' proportions on the mechanical property, water stability, and permeability of solidified glacial debris. Hydration and consolidation mechanisms were analyzed based on XRD and SEM test results. The results indicate that the mechanical properties of solidified glacial debris with the new composite curing agents A, B, and C are superior to those with cement. The permeability coefficients of the solidified glacial debris with 7% dosage of the new composite curing agents A, B and C are both less than 1×10^{-6} cm/s. The reaction between the new composite curing agents and the glacial debris generates crystalline product ettringite (AFt) and gel-like hydration product calcium silicate hydrate (C-S-H). These products enhance interparticle bonding and fill the voids among the glacial debris, which is the main source of strength for the solidified glacial debris. These new composite curing agents provide important reference value for addressing and preventing surface glacial debris collapse.

Keywords: Pulang Copper Deposit; new curing agents; glacial debris consolidates; properties of the consolidated body; consolidation mechanism

check for updates

Citation: Zeng, Q.; Feng, X.; Ren, H.; Sui, S.; Wang, S.; Sun, W.; Liu, J. The Impact of New Composite Curing Agents on the Curing Properties of Glacial Debris in the Pulang Copper Deposit. *Buildings* **2023**, *13*, 2189. https://doi.org/10.3390/buildings13092189

Academic Editors: Andrea Petrella and Chenggao Li

Received: 28 May 2023
Revised: 30 July 2023
Accepted: 18 August 2023
Published: 28 August 2023

Copyright: © 2023 by the authors. Licensee MDPI, Basel, Switzerland. This article is an open access article distributed under the terms and conditions of the Creative Commons Attribution (CC BY) license (https://creativecommons.org/licenses/by/4.0/).

1. Introduction

The Pulang Copper Deposit is a large porphyry copper deposit located in the northeast of Shangri-La City, Diqing Tibetan Autonomous Prefecture, northwest Yunnan Province. It is a typical representative of large porphyry copper deposits [1–4]. In this mining area, the formation lithology is relatively single, the ore reserves are large, the ore material composition is simple and the ore grade is low, the ore body is thick and shallow, the inclination is almost vertical, and the ore body has good overall collapsibility and continuity, and can form continuous caving; thus, natural caving mining can be adopted for mining [5–8]. Natural caving mining is a process whereby rock mass caving occurs with the help of gravity. This process occurs in the excavation space, whereby the weak structural plane of the ore body itself, under the influence of gravity and secondary tectonic stress, gradually breaks and begins to cave. The appropriate amount of ore is released, causing the upper ore rock to cave until the final stage or surface collapse [9–13]. The mining area exhibits a general westward inclination, with a noticeable high-northwest and low-southeast

topography. Following the natural caving of the underground ore body, the overall topography of high-northwest and low-southeast remains unchanged. Moreover, the surface of the mine caving area is covered with thick glacial debris; during the natural caving mining process, the surface collapses to a certain extent, causing the surface glacial debris layer to deform and crack, forming a collapse pit. This pit provides favorable conditions for the formation of underground glacial debris recharge debris flow. During times of continuous heavy rainfall, the surface glacial debris become saturated with water, transitioning from a naturally consolidated dry state to a fluid state. Consequently, they flow into the mine outlet under the force of gravity, resulting in debris flow disasters [14,15]. These disasters significantly impede the safe production of Pulang Copper Mine. Therefore, it is essential to carry out in situ grouting to consolidate the surface glacial debris in the mining area, forming a water-resistant consolidated layer with sufficient mechanical strength. This measure ensures the safe production of the mining area.

Currently, the majority of research on glacial debris conducted both domestically and internationally focuses on the geomorphology of glacial debris, the engineering properties of glacial debris, and the causes and prevention of natural geological debris flow disasters caused by surface glacial debris [16,17]. Within the field of loose accumulation strengthening in engineering work environments, the flower tube grouting method is highly regarded. Zhang Yufang et al. [18] conducted a study on the application and effectiveness of multi-stage grouting steel pipe pile group structural reinforcement technology on slopes. Ma Xiangfeng et al. [19] conducted a study on the deformation behavior of roadbeds and the application of steel pipe grouting reinforcement technology in sand and gravel strata through numerical simulation and field data monitoring and analysis. Their research achieved a relatively ideal reinforcement effect. However, these results primarily focus on grouting technology research, with the grouting process primarily applied to loose accumulation bodies. Currently, there is a lack of research on grouting technology and grouting materials in different dense geological conditions, particularly regarding grouting materials suitable for the characteristics of glacial debris. On the other hand, research on curing agents for consolidating common soil and wind-blown sand has made significant progress, with numerous research findings available [20–22]. Traditional materials such as lime and cement are widely used as components of these curing agents for soil reinforcement. However, when applied to the surface layer of glacial debris in the mining area of Pulang Copper Deposit, these materials exhibit notable limitations and drawbacks, including poor injectivity, low strength of the consolidated body, and inadequate water stability.

Glacial debris is a non-stratified glacial sedimentary soil composed of clay, silt, sand, gravel, and drift materials. Its mineral composition primarily consists of silicate minerals such as quartz, feldspar, and chlorite, with SiO_2 and Al_2O_3 as the main chemical components. Long-term geological conditions have led to significant weathering of glacial debris' mineral constituents, resulting in the presence of amorphous minerals with certain hydration activity [23]. In terms of physical properties, glacial debris is characterized by a wide grain gradation, highly uneven particle sizes, a lack of sorting, high compactness, complex structure, occasional local overhead phenomenon, and large differences in mechanical characteristics [24–26]. Consequently, the surface layer formed by glacial debris deposition exhibits low porosity, small void diameters, and a significant presence of gravel, which further contributes to the non-uniformity of the glacial debris. Therefore, an effective grouting curing agent should possess high injectivity and the ability to hydrate with the amorphous mineral components on the surface of the glacial debris. This will enable the glacial debris components to undergo gelation, thus improving the strength and water stability of the consolidated body.

According to the surface characteristics and engineering requirements of the glacial debris in Pulang Copper Deposit, Yunnan, China, three compound glacial debris curing agents were developed by adjusting the composition materials of cement-based curing agents. The rheological properties of these curing agents, which impact in situ grouting,

were evaluated. Additionally, engineering properties such as the shear resistance, water stability, and permeability of the consolidated glacial debris body were tested. Microcosmic tests were conducted to analyze the mechanism of hydration and consolidation, thereby assessing the gelling effect of the curing agent on the glacial debris. This research offers a cost-effective solution to address the issue of debris flow resulting from surface glacial debris collapse in the mining area of Pulang Copper Deposit. Furthermore, it provides a theoretical foundation for the research and development of glacial debris curing agents and performance optimization.

2. Materials and Methods

2.1. Experimental Materials

(1) Glacial debris

The glacial debris used in the experiment was collected from the surface of the Pulang Copper Deposit in Yunnan Province. X-ray fluorescence spectroscopy (XRF) was used to analyze the chemical composition of the glacial debris, as shown in Table 1. The analysis was conducted using a wavelength-dispersive X-ray fluorescence (WDXRF) spectrometer from Shimadzu Corporation in Japan. The total chemical composition of the glacial debris added up to 100%, excluding combustion losses.

Table 1. Chemical composition of glacial debris (%).

Composition	Na_2O	MgO	Al_2O_3	SiO_2	P_2O_5	SO_3	Cl	K_2O	CaO	TiO_2	Cr_2O_3
mass fraction	1.91	3.96	18.94	56.1	0.93	0.16	0.04	4.99	2.79	1.02	0.02
Composition	MnO	Fe_2O_3	CuO	ZnO	Rb_2O	SrO	Sc_2O_3	ZrO_2	BaO	NiO	Total
mass fraction	0.06	8.61	0.11	0.01	0.03	0.13	0.01	0.06	0.11	0.01	100

The glacial debris used is shown in Figure 1. Soil testing was performed on the glacial debris in accordance with GB/T 50123-2019 to determine its density and moisture content, as shown in Table 2. Figure 2 shows the grain gradation curve. The glacial debris is well graded, with a particle inhomogeneity coefficient C_u of 11.29 (>5) and a particle curvature coefficient C_v of 1.22 (falling between 1 and 3).



Figure 1. Glacial debris.

Table 2. Basic physical properties of glacial debris.

Wet Density (kg/m^3)	Dry Density (kg/m^3)	Moisture Content (%)
2.29×10^3	2.21×10^3	11.83

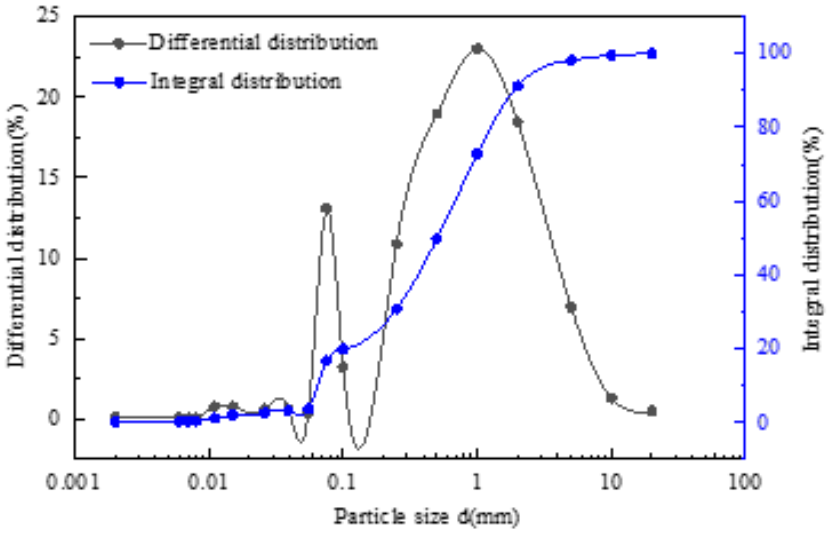


Figure 2. Grain gradation curve for Glacial debris.

(2) Curing agent

The consolidating agent used in this study is a cementitious consolidating material composed of cement, lime, gypsum, slag, and surfactant, as presented in Table 3, which shows the chemical composition of each raw material. The ordinary Portland cement type Jidong P.O.42.5 was selected for the test, and its basic properties are presented in Table 4. During the test, consolidating agents A, B, and C were comparatively evaluated with cement, and the curing agent mixing ratios are shown in Table 5.

Table 3. Main chemical composition of the raw materials (%).

Materials	CaO	SiO_2	SO_3	MgO	Al_2O_3	Fe_2O_3	K_2O	Na_2O	MnO_2	LOI	Total
Cement	62.40	21.55	1.64	2.17	5.68	3.69	0.62	-	-	2.25	100
Lime	97.04	-	-	-	-	-	-	-	-	-	97.04
Gypsum	33.57	2.45	41.03	0.55	1.21	0.61	0.67	0.72	-	18.66	99.47
Slag	38.22	32.87	-	8.4	11.48	0.48	6.82	-	0.11	1.04	99.42

Table 4. Main performance indexes of cement.

Specific Surface Area (m^2/kg)	Initial Setting Time (min)	Final Setting Time (min)	Stability	Loss (%)	Compressive Strength	
					3 d (MPa)	28 d (MPa)
342	201	256	Qualified	2.25	26.4	50.8

Table 5. Curing agent mix ratio.

Curing Agents	Cement	Lime	Gypsum	Slag	Surfactant
cement	100	0	0	0	0
A	30	48	6	16	0.6
B	35	43	6	16	0.6
C	40	38	6	16	0.6

2.2. Experimental Methods

2.2.1. Experimental Scheme

Table 6 shows the specific curing scheme for the control group and several experimental groups, which utilized cement solidified glacial debris as a reference. The curing agent

content was varied using mass ratio gradients of 5%, 7%, 9%, 11%, and 13%, and samples of the glacial debris consolidated body were prepared accordingly. For instance, the glacial debris body consolidated with a 5% content of curing agent A is labeled as A05.

Table 6. Curing scheme.

Sample Code	Glacial Debris	Curing Agent				Water
		A	B	C	Cement	
A05	84	4	0	0	0	12
A07	82	5.5	0	0	0	12.5
A09	80	7	0	0	0	13
A11	78	8.5	0	0	0	13.5
A13	76	10	0	0	0	14
B05	84	0	4	0	0	12
B07	82	0	5.5	0	0	12.5
B09	80	0	7	0	0	13
B11	78	0	8.5	0	0	13.5
B13	76	0	10	0	0	14
C05	84	0	0	4	0	12
C07	82	0	0	5.5	0	12.5
C09	80	0	0	7	0	13
C11	78	0	0	8.5	0	13.5
C13	76	0	0	10	0	14
Cement05	84	0	0	0	4	12
Cement07	82	0	0	0	5.5	12.5
Cement09	80	0	0	0	7	13
Cement11	78	0	0	0	8.5	13.5
Cement13	76	0	0	0	10	14

In accordance with the Standard of Geotechnical Test Method GB/T 50123-2019, the compressive strength of the glacial debris consolidated body was measured after curing, and the optimal ratio scheme of the curing agent was determined. The influence of the curing agent on the shear, water stability, impermeability, and other properties of glacial debris was then studied using cement-solidified glacial debris as the control group, and its microscopic mechanism was analyzed.

2.2.2. Fluidity Test

The fluidity of the slurry was tested following the guidelines of GB/T8077-2012, which outlines the test method for the uniformity of concrete admixtures.

2.2.3. Strength Test

The glacial debris, curing agent, and water were mixed and stirred according to the curing plan in Table 6. The resulting mixture was then loaded into 40 mm × 40 mm × 40 mm test molds to undergo curing and solidification. To simulate the project site environment, the cured glacial debris was kept indoors at a temperature of 20 ± 2 °C and a relative humidity of 60%~80% for 3 days, 7 days, 28 days, and 56 days. The compressive strength of the cured glacial debris was tested in accordance with the Standard for Geotechnical Test Methods GB/T 50123-2019.

2.2.4. Shearing Test

Variable angle shear testing was adopted in this test due to the high strength of cured glacial debris. In accordance with the current standards of DZ/T 0276.25-2015, the "Test code for physical and mechanical properties of rocks Part 25: Shear strength test of rocks [S]", samples measuring 70 mm × 70 mm × 70 mm were prepared. The samples were kept indoors for 4, 14, and 28 days under natural ventilation conditions. After the samples

reached the corresponding curing time, shear fixtures of 20°, 30°, and 45° were used to conduct variable angle shear tests on the cured glacial debris samples.

2.2.5. Water Stability Test

In accordance with the current standards of CJ/T 486-2015 "Soil Curing Admixture", standard samples measuring Φ50 mm × 100 mm were prepared. The water stability of the glacial debris was evaluated by adopting the ratio of the unconfined compressive strength of the stability sample soaked in water on the last day of the standard curing period of 7 days to the unconfined compressive strength of the test specimen of the same age without soaking in water. This ratio was used as the coefficient of water stability.

2.2.6. Permeability Test

Due to the relatively small permeability coefficient of solidified glacial debris and the limited permeability quantity after being strengthened by the curing agent, the constant head permeability test yielded a large error. Therefore, the variable head permeability test was adopted to measure the permeability coefficient. Preparation and maintenance were carried out according to GB/T 50123-2019 "Standard for Geotechnical Test Methods", and the permeability coefficient was measured after 7 d of curing.

2.2.7. Microanalysis

To investigate changes in the mineral composition of the reinforced glacial debris before and after curing material treatment, all samples to be tested underwent X-ray diffraction (XRD) analysis after being ground and passed through a 0.045 mm square hole screen. A 9 kW Smartlab X-ray diffractometer (from Rigaku Corporation, Akishima, Japan) with a copper target was used to conduct the XRD analysis, with samples placed in a special sample box, compacted, and smoothed prior to scanning.

Scanning electron microscopy (SEM) was utilized to investigate the microstructure morphology of the curing agent and cement-cured glacial debris after undergoing standard curing for 28 days.

2.3. Flowchart of the Paper

The Flowchart of the paper is shown in Figure 3.

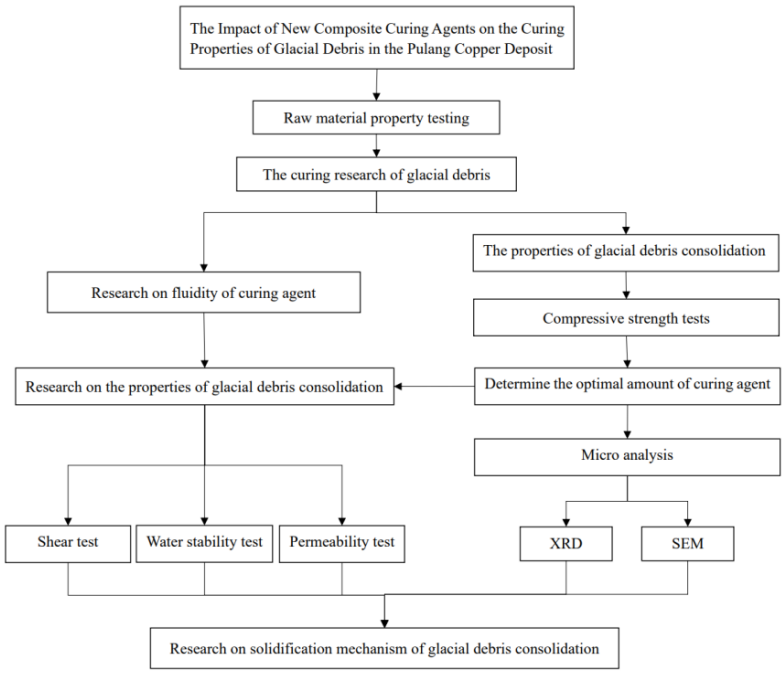


Figure 3. Flowchart of the paper.

3. Results and Analysis

3.1. Study on the Fluidity of the Curing Agents

To investigate the fluidity of the curing agent and cement, separate tests were conducted for each. Figure 4 demonstrates the fluidity measurements of curing agents A, B, and C, and cement, respectively. As illustrated in the figures, the fluidity of curing agents A and B was slightly higher than that of cement, whereas the fluidity of curing agent C was slightly lower. However, the differences in fluidity among A, B, C, and cement were negligible, indicating that they all meet the requirements for grouting.

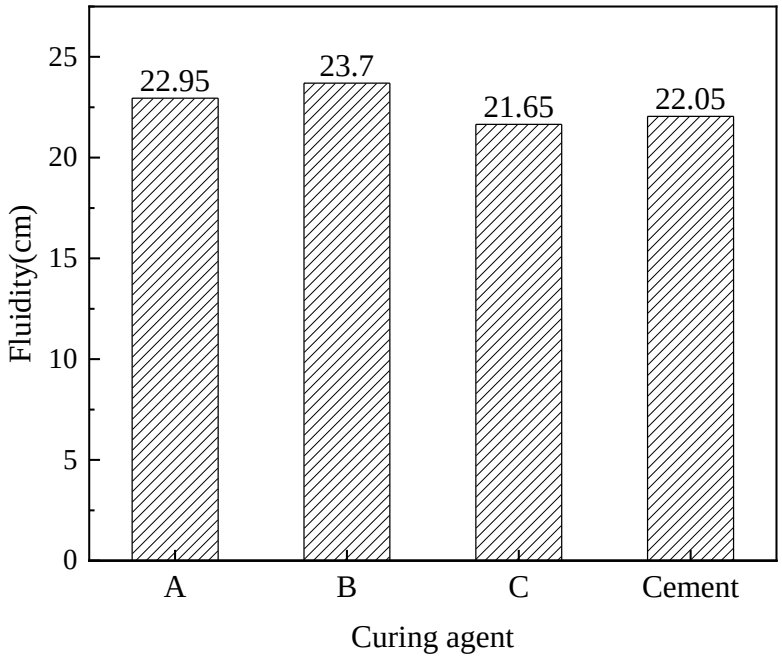


Figure 4. Fluidity of different curing agents.

To investigate the microscopic fluidity of cement and curing agents A, B, and C, four curing materials were tested for their Zeta potential values, as illustrated in Figure 5. As shown in the figure, the Zeta potential of curing agents B and A was higher than that of cement, while the Zeta potential of curing agent C was lower. Zeta potential is a measure of the strength of mutual repulsion or attraction between particles, with higher absolute values indicating the greater system stability and better fluidity of the cementing material [27–29]. Thus, of the four curing agents tested, curing agent B exhibited the highest fluidity, with both curing agents A and B displaying better fluidity than cement. These findings indicate that curing agents are able to disperse more effectively among glacial debris particles than cement, with curing agent B demonstrating the most effective dispersion and promoting superior curing results. These results are consistent with the findings of macroscopic solidified material flow tests.

3.2. The Effect of Different Curing Agents on the Compressive Strength of the Glacial Debris Consolidated Body

The influence of the dosage of curing agent on the compressive strength of the glacial debris consolidation body is shown in Figure 6. It can be seen from Figure 6 that the compressive strength of the solidified glacial debris with curing agents A, B and C at different ages is higher than that of cement, and its compressive strength is positively related to the amount of solidified agent. The strength of solidified glacial debris with curing agents A, B and C in a lower amount is far higher than that of the solidified glacial debris with a higher amount of cement. According to Figure 6, it can be seen that the compressive strength of some glacial debris consolidated bodies decreased to varying

degrees between 3–7 days and 28–56 days. The reasons for this decrease were analyzed, and it is believed that the decrease in strength after 3–7 days of maintenance may be due to the short interval time and the insignificant increase in strength. This is due to the fact that in order to approach the actual conditions of the project, the sample is cured in low-humidity air, which can cause loss of moisture in the sample. With the increase in curing age, obvious cracks appear on the surface of the sample after 28 days, so it is considered that the strength of the consolidation body of the glacial debris will not increase significantly after 28 days, but the appearance of cracks leads to a reduction in strength.

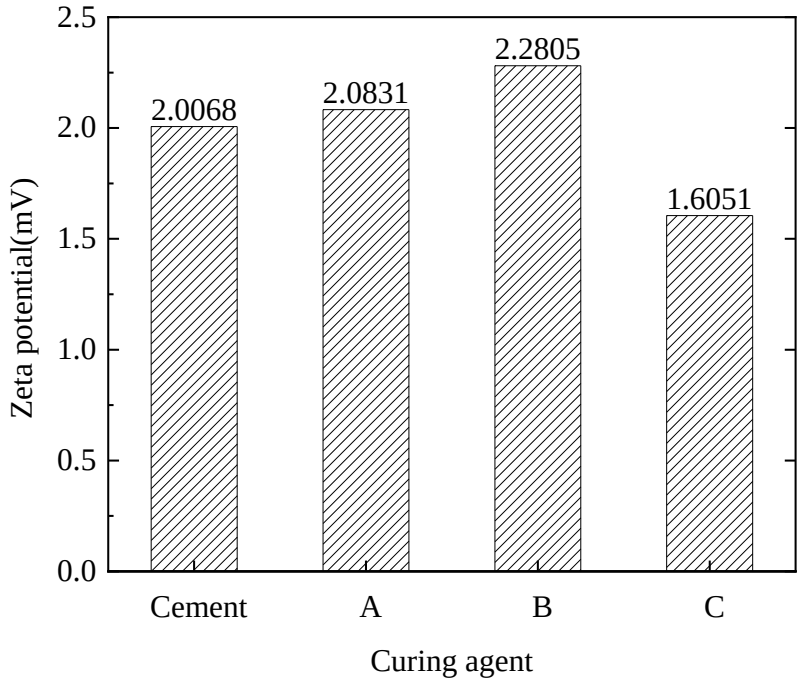
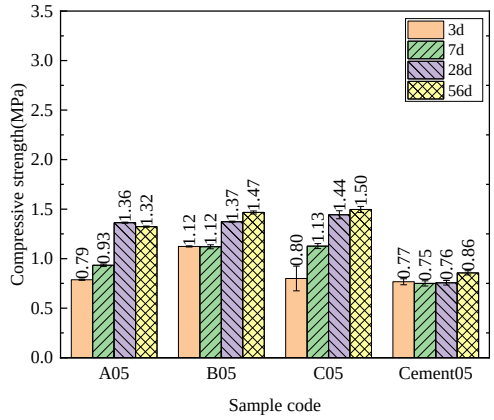
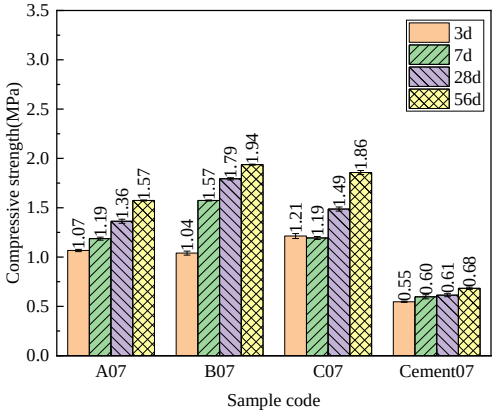


Figure 5. Zeta potential of different curing agents.

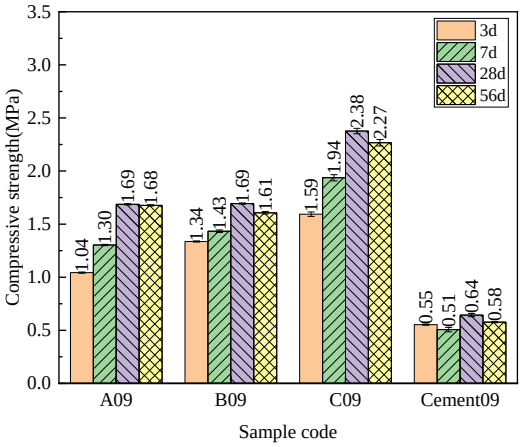
From the solidification effect of three kinds of curing agents and cement, the strength of the glacial debris body consolidated with the new curing agent is significantly higher than that of cement body consolidated at the same dosage. Moreover, with the increase in the content, the strength of the glacial debris consolidated by the new curing agent shows a significant increasing trend, but the strength of the cement consolidated body has no obvious increase trend. The reason for this effect is mainly related to the composition and structure of clay minerals in glacial debris. The main mineral components of glacial debris are silicate minerals such as quartz and feldspar. Under geological action, these minerals are partially weathered to form amorphous components, which have dissolution characteristics in an alkaline environment. When encountering Ca $(OH)_2$ and $CaSO_4 \cdot 2H_2O$ components, hydration products such as C-S-H and AFt will be generated, forming a certain cementation strength. The generation of hydration products can be increased to a certain extent by properly increasing the amount of lime and gypsum. This will be beneficial for improving strength. After the pure cement is mixed with till, the hydration products of the cement wrap the clay particles to make the glacial debris consolidated body produce a certain strength; however, the clay particles have the characteristics of high dispersion and expansion when encountering water [30,31], which causes the strength of cement consolidated glacial debris to be low, and the strength does not change significantly with an increase in the dosage.



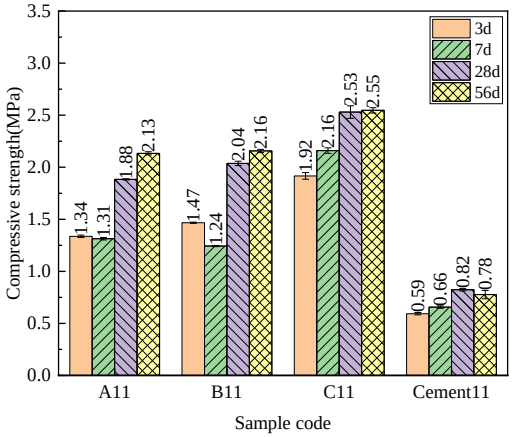
(**a**)



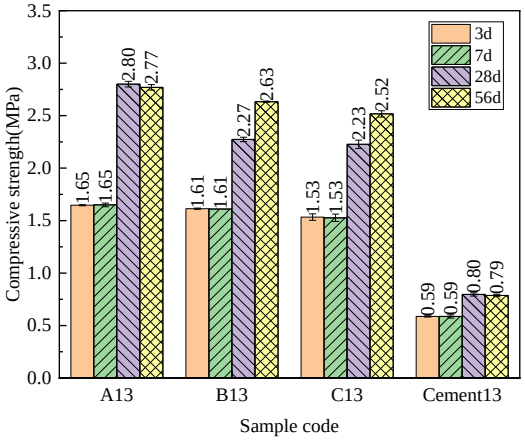
(**b**)



(**c**)



(**d**)



(**e**)

Figure 6. Influence of curing agent dosage on the compressive strength of glacial debris consolidation: (**a**) with 5% dosage; (**b**) with 7% dosage; (**c**) with 9% dosage; (**d**) with 11% dosage; (**e**) with 13% dosage.

From the impact of the new curing agent on the strength between different sample groups, it can be seen that the curing agent corresponding to the highest-strength consolidation body is not fixed at different dosages. When the dosage of the curing agent is 5%, there is no significant difference between curing agents A, B, and C. When the dosage is 7%,

the curing effect of curing agent B is better; when the dosage is 9% and 11%, curing agent C shows obvious advantages. When the yield is 13%, the curing effect of curing agent A is the best. This is because the curing agent developed in this article is mixed with a certain amount of lime, gypsum, and slag powder. Amorphous SiO_2 and Al_2O_3 components dissolved in glacial debris can react with lime and gypsum to produce C-S-H and Aft [32], and produce strength. At the same time, the auxiliary cementitious effect of slag also has a certain impact on the strength. However, there must be an optimal corresponding value between lime, gypsum and amorphous SiO_2 and Al_2O_3 components. This corresponding value affects the strength of the glacial debris consolidation body when the dosage of curing agent is different.

According to the analysis of the above strength results, the strength of glacial debris consolidation body when the new type of consolidation agent is added at 7% can meet engineering needs, and the corresponding amount of cement as the consolidation agent needs to reach 11%. Therefore, in the subsequent experiments, a curing scheme with 7% of curing agent A, B and C and 11% of cement was selected as for comparison to further study the bending resistance, shear resistance, water stability, permeability, and other properties of the glacial debris consolidation body.

3.3. The Effect of Different Curing Agents on the Shear Performance of the Glacial Debris Consolidated Body

A variable angle shear test was adopted in this experiment, and the shear samples of cured glacial debris were prepared using the proportions and dosages of curing agents mentioned above. The curves of cohesion and the internal friction angles of the cured glacial debris varying with age were obtained, as shown in Figures 7 and 8. It can be seen from the Figures that the cohesion and internal friction angle of the glacial debris solidified with 7% curing agents A, B, and C and 11% cement both increased with age. Moreover, the cohesion and internal friction angle of the glacial debris solidified with 7% curing agents A, B, and C were higher than those of the glacial debris solidified with 11% cement. With the increase in curing time, the cohesion of the glacial debris solidified with 11% cement increased slowly at first, and then quickly. In contrast, the cohesion of the glacial debris solidified with 7% curing agents A, B, and C increased rapidly in the early stage, and the growth rate showed a downward trend in the later stage. The curing agent utilized contains a significant amount of lime, which contributes to a considerable amount of $Ca(OH)_2$ in the early stages of the reaction. This provides an alkaline environment that promotes the reaction between cement and slag, producing a plethora of hydration products that improve the early-stage cohesion of the solidified glacial debris. Conversely, the cement system's reaction is relatively slow, occurring gradually with increased age. In comparison to the curing agent, its primary contribution to the glacial debris' cohesion occurs later in the reaction process.

3.4. The Effect of Different Curing Agents on the Water Stability of the Glacial Debris Consolidated Body

Samples of cured glacial debris were prepared using the proportions and dosages of curing agents mentioned above, and the corresponding water stability coefficient of the solidified glacial debris was obtained, as shown in Figure 9. From Figure 9, it can be observed that the water stability coefficient of the glacial debris solidified with 7% curing agents A, B, and C was slightly lower than that of the glacial debris solidified with 11% cement. However, all the samples met the engineering requirements for water stability. Among the three curing agents, curing agent B resulted in the best water stability, which was slightly better than that of curing agents A and C.

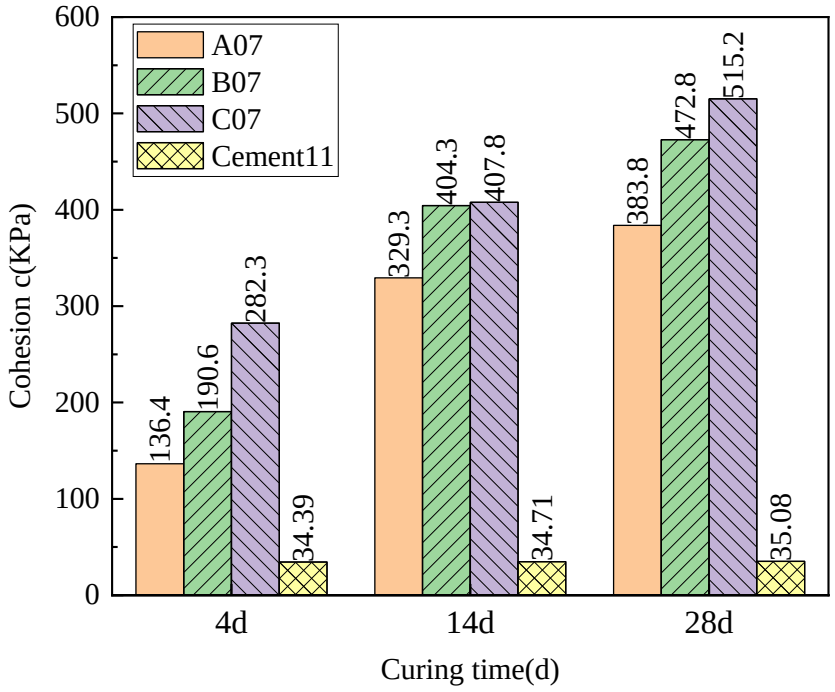


Figure 7. Influence of different curing agents on the cohesion of glacial debris consolidation.

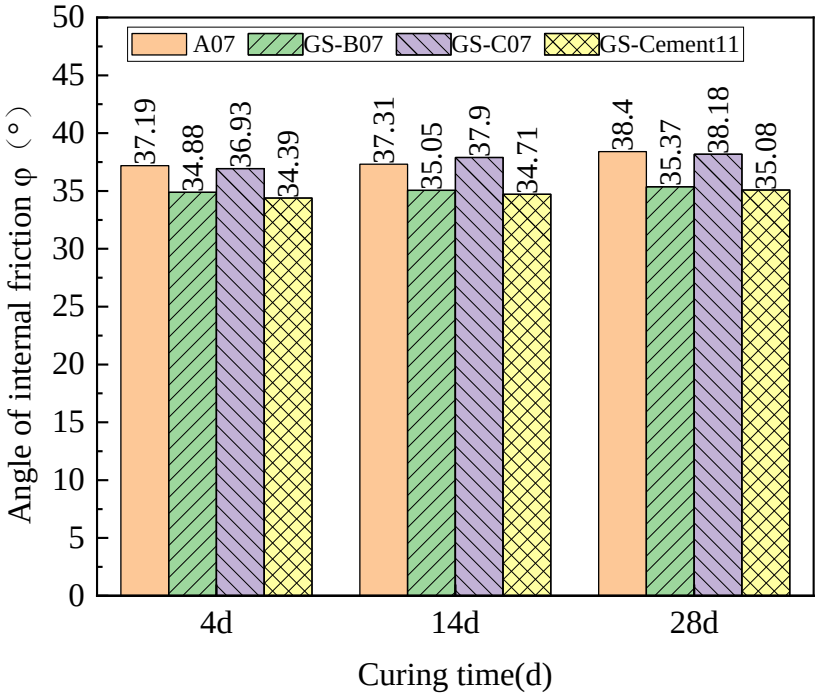


Figure 8. Influence of different curing agents on the friction angle of glacial debris consolidation.

3.5. The Effect of Different Curing Agents on the Permeability of the Glacial Debris Consolidated Body

Samples of cured glacial debris were prepared using the proportions and dosages of curing agents mentioned above, and the permeability test was conducted on the samples solidified with 7% dosage of curing agents A, B and C, respectively. The permeability coefficient of the cured glacial debris was measured after 7 days of curing, and the test results were shown in Figure 10. As can be seen from Figure 10, the permeability coefficients of the samples solidified using curing agents A, B and C were both less than 1×10^{-6} cm/s.

By consulting the data, it was found that the permeability coefficient of cement-cured glacial debris is generally m $\times$ 10^{-6} cm/s ($1 \leq m < 10$). In practical application, the permeability coefficient K of a considerable part of cement glacial debris-impervious engineering is m $\times$ 10^{-5} cm/s ($1 \leq m < 10$), which still has a good impervious effect. Therefore, it can be inferred that the glacial debris samples solidified with curing agents A, B and C have good impermeability, and can meet the actual construction requirements.

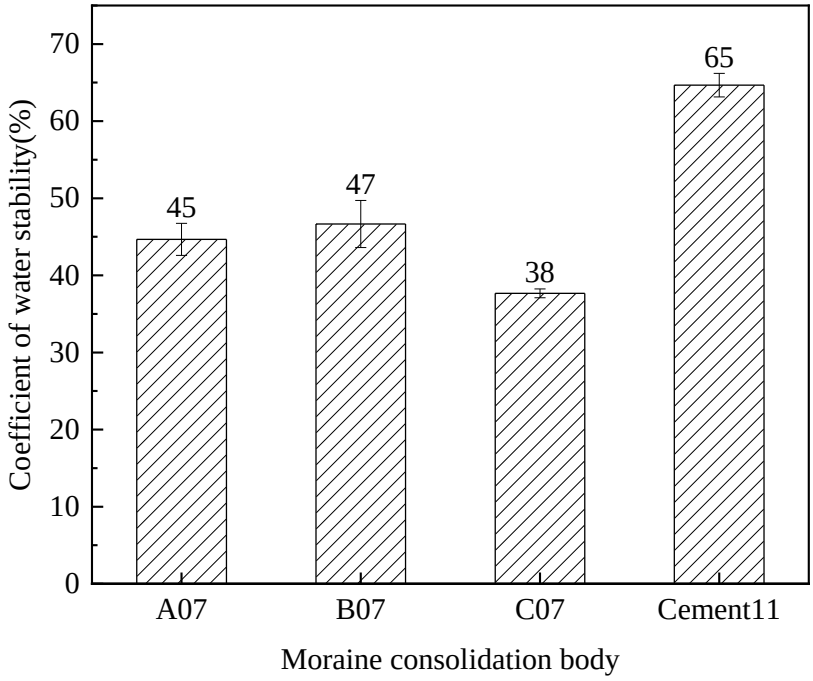


Figure 9. Water stability coefficient of glacial debris solidified using different curing agents.

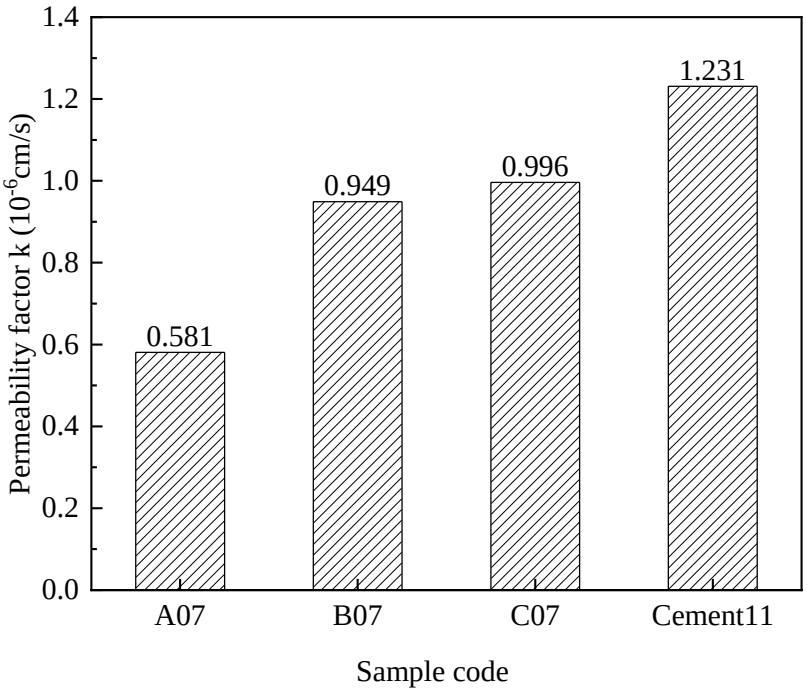
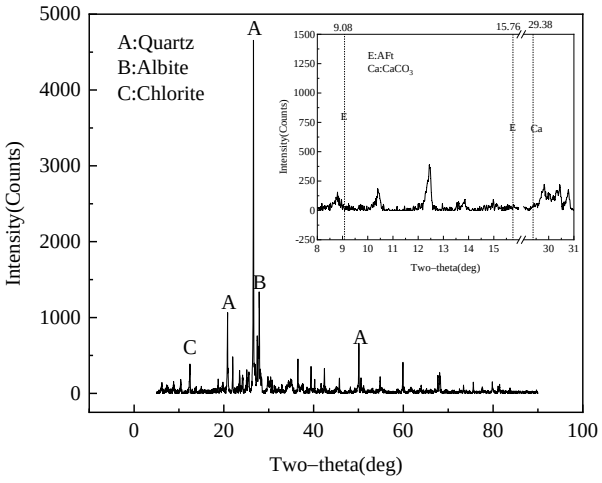


Figure 10. Influence of different curing agents on the permeability of glacial debris consolidation.

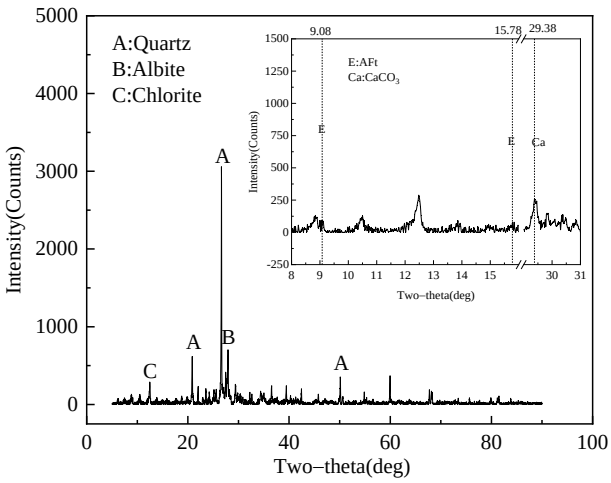
3.6. Microscopic Test

3.6.1. XRD Analysis

Figure 11 displays the diffraction pattern and material composition of the till before and after consolidation. According to the analysis of the test results, the main mineral components of the glacial debris were aluminosilicate minerals such as quartz, albite and chlorite. Three different curing agents of 7% and 11% cement were added to solidify the glacial debris. The XRD patterns of the samples before and after solidification were compared and analyzed. In the cured glacial debris, the diffraction peak intensity of quartz, albite and chlorite was significantly reduced, especially that of albite. Meanwhile, in the cured glacial debris, weak ettringite (AFt) diffraction characteristic peaks appeared near the positions with 2θ angles of 9.08° and 15.78° [33,34], and obvious calcium carbonate diffraction characteristic peaks appeared at the positions with 2θ angles of 29.38° [35], indicating that AFt, a hydration product, was generated in the cured glacial debris formed by four different curing schemes. In addition, some of the $Ca(OH)_2$ released by the consolidation agent or cement hydration in the hydration process is carbonized, and $CaCO_3$ is generated. In addition, it can be seen from the comparison between the intensity reduction of the characteristic peaks of main minerals in the glacial debris and the intensity of the characteristic peaks of the newly emerged hydration products (AFt) that there is a big difference between them. The decrease in the characteristic peak intensity of the main minerals was much greater than the characteristic peak intensity value increase in the newly generated phase, and the hydration products generated by the reaction consumption of quartz components and albite minerals were not shown in the XRD pattern, indicating that a large number of amorphous hydration products were also formed in the system [32]. These crystalline hydration products played the role of skeleton support in the solidified body of the glacial debris. Amorphous hydration products strengthened the bonding force among the glacial debris particles, enhanced its cementation, and filled the pores among the glacial debris particles.

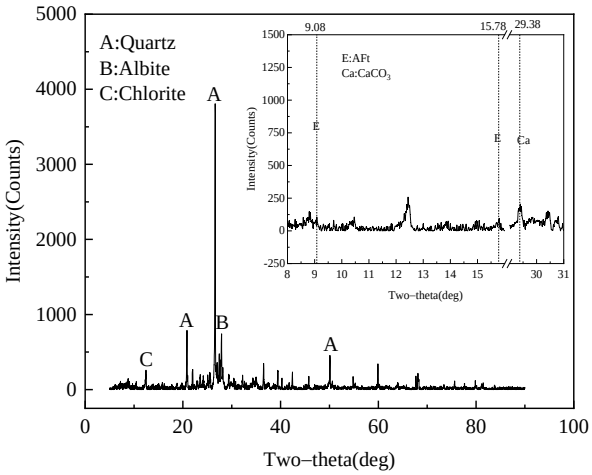


(**a**)

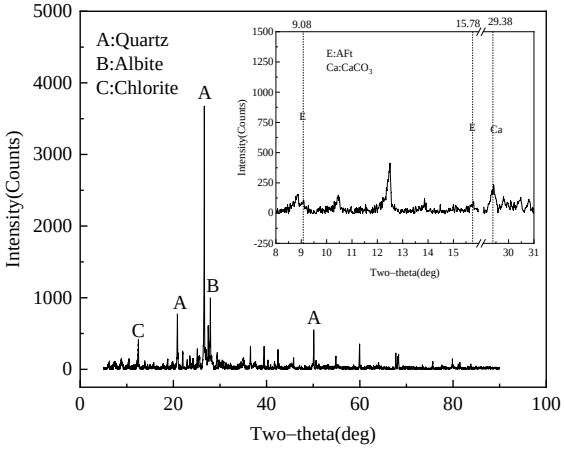


(**b**)

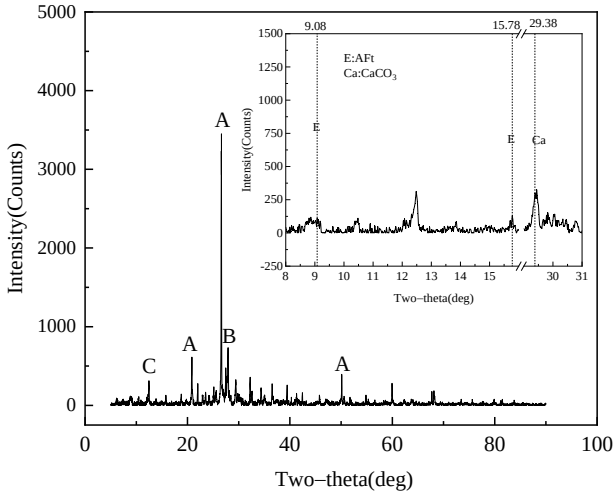
Figure 11. *Cont.*



(**c**)



(**d**)



(**e**)

Figure 11. XRD patterns of the glacial debris cured using different curing agents: (**a**) natural glacial debris; (**b**) A07; (**c**) B07; (**d**) C07; (**e**) Cement11.

3.6.2. SEM Analysis

SEM analysis of the glacial debris body consolidated with 7% curing agent B and the glacial debris body consolidated with 11% cement were conducted, and their respective SEM images were obtained, as shown in Figure 12. The SEM image of the curing agent B-solidified glacial debris after 28 days shows a relatively dense internal structure with a uniform distribution of glacial debris particles. The solidified products are tightly bound around the glacial debris particles, and no obvious voids, holes or cracks can be observed in the internal structure, despite the 30% water content of the test block. Consequently, the solidified glacial debris exhibits improved strength and deformation resistance and is less prone to slip under external forces. The cement solidified glacial debris after 28 days exhibits a relatively loose internal structure, with visible gaps and holes between the cement and soil particles.

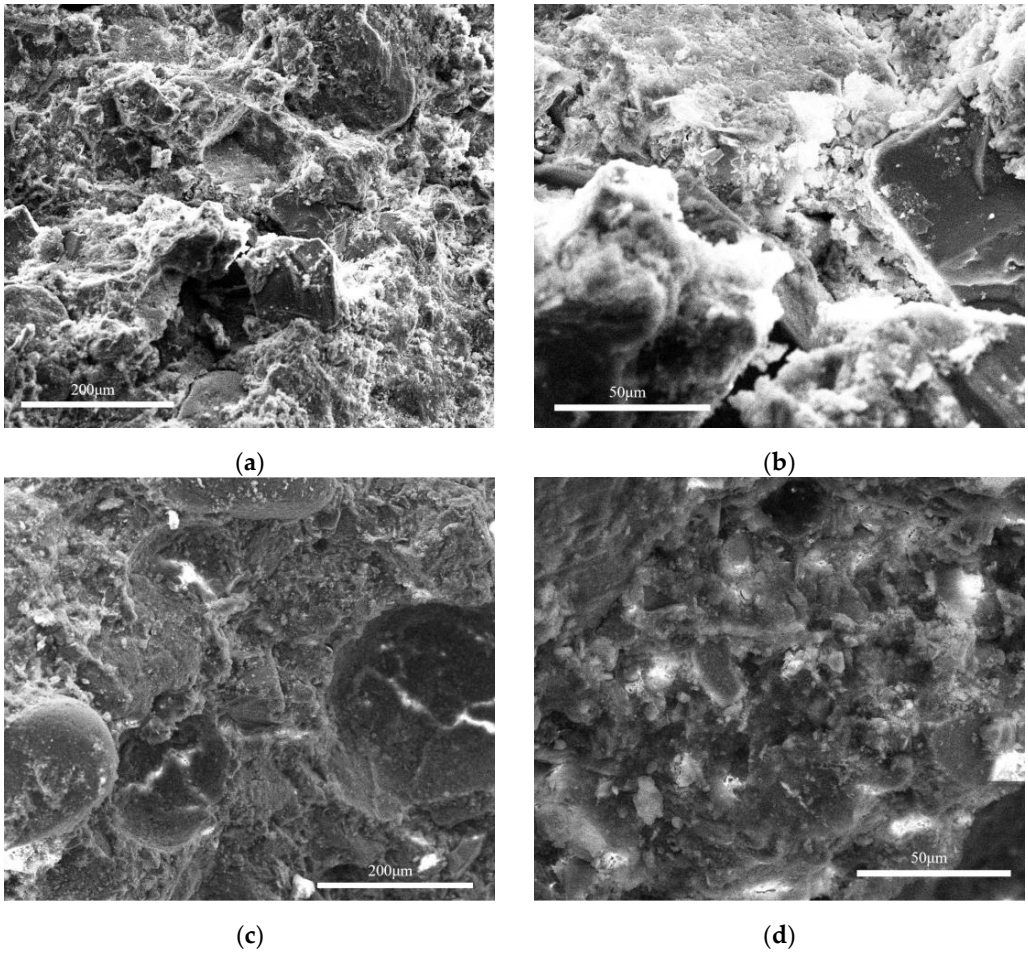


Figure 12. SEM analysis of the glacial debris cured using different curing agents: (**a**) Cement11, magnification = ×500; (**b**) Cement11, magnification = ×2000; (**c**) B07, magnification = ×500; (**d**) B07, magnification = ×2000.

4. Conclusions

Compressive, shear, water stability, permeability, and microscopic tests were conducted on glacial debris cured with three kinds of curing agents A, B, C, and cement, in order to comprehensively evaluate the curing properties of curing agents A, B, and C and study and analyze the curing mechanism. The following conclusions were drawn:

1. Through a large number of compressive strength tests on the glacial debris body solidified using different proportions of curing agents, it can be concluded that curing agents A, B, and C can achieve good curing effects, and all indicators can meet the requirements of engineering construction. Taking cost into consideration, Three optimal schemes of curing agents A, B and C with a content of 7% were initially selected.
2. An XRD and SEM microscopic analysis of the cured glacial debris showed that the three curing agents and cement generated AFt and C-S-H gel through their hydration reactions in the process of curing the glacial debris. The crystalline hydration products were used to establish a supporting skeleton in the cured glacial debris system. The gelatinous hydration products acted as the cement among the glacial debris particles and filled the pores among the glacial debris particles, thus improving the engineering properties of the glacial debris and solving the ore dilution caused by the caving mining of Pulang Copper Deposit and the debris flow formed by the collapse of the glacial debris.

3. During the research and development of solidifying agents, the application of a multi-component curing material ratio scheme can yield a synergistic effect by leveraging the combined properties of multiple components. This approach effectively enhances the activity of the target material, resulting in a more substantial curing effect. Furthermore, it compensates for the limitations and deficiencies of using a single curing agent in practical engineering applications. These findings provide crucial insights for the further investigation of glacial debris hardeners.

Author Contributions: Resources, Q.Z.; Data curation, Q.Z.; Supervision, X.F.; Formal analysis, X.F.; Writing—original draft, H.R.; Project administration, S.S.; Validation: S.S.; Investigation, S.W.; Methodology, W.S.; Conceptualization, J.L. All authors have read and agreed to the published version of the manuscript.

Funding: This research received no external funding.

Data Availability Statement: Not applicable.

Conflicts of Interest: The authors declare no conflict of interest.

References

1. Chen, L.; Pan, L.; Huang, F.; Xu, J.F. Magma Mixing in the Giant Pulang Porphyry Copper Deposit, Yunnan Province: Evidence from Melt Inclusions. *Geotecton. Metallog.* **2018**, *42*, 880–892. [CrossRef]
2. Zhang, S.Y.; He, W.Y.; Gao, X.; Zhang, H.R.; Yuan, J.J. Ore-forming fluids evolution of the porphyry Cu deposits: Alteration mineralogy and thermodynamic modeling of the Pulang Cu deposit, Zhongdian district. *Acta Petrol. Sin.* **2020**, *36*, 1611–1626.
3. Guo, D.X.; Liu, X.; Zhang, H.L.; Zhang, Z.G. The Infrared Spectroscopy Characteristics of Alteration and Mineralizationin the Porphyry Copper Deposit in Pulang, Yunnan Province. *Rock Miner. Anal.* **2021**, *40*, 698–709. [CrossRef]
4. Li, W.C.; Zeng, P.S. Characteristics and metallogenic model of the Pulang superlarge porphyry copper deposit in Yunnan, China. *J. Chengdu Univ. Technol. (Sci. Technol. Ed.)* **2007**, *34*, 436–446.
5. Liu, H.W.; Feng, X.L.; Liang, J.B.; Wu, M.; Li, X.H.; Zhao, B.F. Application Research on the Key Technologies of Large-scale Mining in Pulang Copper Mine. *Min. Res. Dev.* **2016**, *36*, 1–5. [CrossRef]
6. Wu, W.H.; Wu, L.R.; Liu, H.W.; Feng, X.L.; Shen, Q.W.; Cao, Y. Research on the Productive Ore Management for Natural Caving Mining Method in Pulang Copper Mine. *Min. Res. Dev.* **2018**, *38*, 46–49. [CrossRef]
7. Xiao, W.G.; Li, Z.R.; Chen, L.; Feng, X.L.; Zhu, J.N.; Liu, H.W.; Li, Q.S. Study on the Formation Technique of the Cutting Shaft by Natural Caving Method of Pulang Copper Mine. *Met. Mine* **2021**, *11*, 64–68. [CrossRef]
8. Liu, H.J.; Peng, P.A.; Wang, L.G. Comprehensive evaluation and simulation for large-scale mining using natural caving method. *J. Cent. South Univ. (Sci. Technol.)* **2015**, *46*, 617–624.
9. Liu, H.W.; Feng, X.L.; Wu, M.; Li, X.H. Simulation Research on Stress Change of Bottom Structure in Pulang Copper Mine. *Min. Res. Dev.* **2016**, *36*, 28–31. [CrossRef]
10. Yu, S.F.; Wu, A.X.; Han, B. Application of Natural Caving Method on the Thick and Broken Orebody. *Met. Mine* **2012**, *9*, 1–4.
11. Zhu, Z.H.; Dai, B.B.; Tao, G.Q.; Feng, X.L. Research and Application Overview of Block Caving Method. *Met. Mine* **2019**, *12*, 1–11. [CrossRef]
12. Liu, Q.; Sha, W.Z.; Wang, P.; Peng, Z.; Cai, Y.S.; Wei, Y.H.; Huang, Z.G. Stability Monitoring and Analysis on Bottom Structure for Natural Caving Mining Method. *Min. Res. Dev.* **2021**, *41*, 31–35. [CrossRef]
13. Sanchez, V.; Castro, R.L.; Palma, S. Gravity flow characterization of fine granular material for Block Caving. *Int. J. Rock Mech. Min. Sci.* **2018**, *114*, 24–32.
14. Fu, J.X.; Tan, Y.Y.; Song, W.D. Study on mechanism of rainfall infiltration through overlying loess formation on block caving collapse area. *J. China Univ. Min. Technol.* **2015**, *44*, 349–353. [CrossRef]
15. Niu, X.D.; Hou, K.P.; Sun, H.F. Experimental Study on the Flow Mechanism of Fine-grained Moraine in the Process of Uniform Ore Drawing. *J. Min. Strat. Control. Eng.* **2023**, *5*, 24–31. [CrossRef]
16. Qu, Y.P.; Tang, C.; Liu, Y.; Chang, M.; Tang, D.S. Investigation and Analysis of Glacier Debris Flow in Nyingchi Area, Tibet. *Chin. J. Rock Mech. Eng.* **2015**, *34*, 4013–4022. [CrossRef]
17. Shen, B.; Ma, D.T.; Wang, Y.Q. Suggestions on identification of Sesiman debris flow and preventive measures of Aba area of Sichuan Province. *Yangtze River* **2013**, *44*, 44–46. [CrossRef]
18. Zhang, Y.F.; Wei, S.W.; Zhou, W.J.; Li, D.W.; Zhou, B. Model test study on anti-sliding behaviours of multiple segmented grouting steel pile group structure. *Chin. J. Rock Mech. Eng.* **2019**, *38*, 982–992. [CrossRef]
19. Ma, X.F.; Wang, L.C.; Gong, L.; Chen, L.B. Deformation and Grouting Reinforcement for Railway Subgrade Crossed by a Double-Track Metro Shield Tunnel in Sandy-Cobble Strata. *Tunn. Constr.* **2021**, *41*, 181–189.
20. Zhang, Y.B.; Zhang, W.C.; Li, Y.S.; Zhao, L.M.; Li, H.Y.; Lei, Y.B.; Yang, Y.Q. Experimental of Consolidation Performance of Laterite in Plateau Based on RSM. *Mater. Rep.* **2023**, *37*, 259–264.

21. Wu, Y.P.; Wang, X.S.; Kim, S.; Wang, Z.H.; Liu, T.Y.; Liu, Y. Experimental study of the working property and strength behavior of waste marine clay with high water content modified with quicklime, ground calcium carbonate, and a WXS-II soil stabilizer. *Constr. Build. Mater.* **2022**, *360*, 129622. [CrossRef]
22. Huang, Y.F.; Fan, W.F.; Wu, J.L.; Xiang, X.L.; Wang, G. Experimental Study on Strength and Microstructure of Glacial Till Stabilized by Ionic Soil Stabilizer. *Buildings* **2022**, *12*, 1446. [CrossRef]
23. Chen, A.D.; Gu, J.N.; Zhao, Z.Z.; Qian, F.; Wang, H.L. Quartz grains SEM surface microtextures of Quaternary glacial sediments along the Diancang Mountain in Yunnan, Southwest China. *J. Glaciol. Geocryol.* **2016**, *38*, 453–462.
24. Yang, D.; Wang, J.C.; Yang, D.X. Moraine slope structure in Parlung Zangbo River Basin and its stability evaluation method. *Yangtze River* **2019**, *50*, 108–112. [CrossRef]
25. Gao, B.; Wang, J.C.; Zhang, J.J.; Chen, L.; Li, Y.L. Analysis of the Development Characteristics of Typical Glacial Debris Flow that has Materials Source of Moraine and Colluvial or Slide Deposits in the Parlung River (Bomi-Suotong). *Sci. Technol. Eng.* **2018**, *18*, 176–182.
26. Yang, D.X.; You, Y.; Wang, J.C.; Yang, D.; Liu, J.K. Characteristics of Typical Glacial Tills in Parlung Zangbo Basin in Southeastern Tibet and Its Engineering Effect. *J. Disaster Prev. Mitig. Eng.* **2020**, *40*, 841–851. [CrossRef]
27. Liu, K.; Cai, J.S.; Mu, S.; Zhang, H.; Ma, Q.; Liu, G.Y. Study on the effect of synergist on the properties of cement. *Concrete* **2023**, *3*, 69–73.
28. Ma, X.T.; Wan, G.X.; Zhen, X. Influence of metal ions on fine slime cover in coal flotation. *Coal Eng.* **2023**, *55*, 167–172.
29. Hou, Y.Y.; Zeng, X.H.; Long, G.C.; Xie, Y.J.; Xiao, B.C.; Gu, Y.H.; Dong, H.Z.; Pan, Z.L.; Zhao, W.Q.; Yang, J.F. Rheological Properties of Natural Pozzolan-Cement-Fly Ash Composite Slurry. *Mater. Rep.* **2022**, *36*, 97–102.
30. Fan, H.H.; Wu, P.T.; Li, P.; Jia, L.; Zhang, S. Study on identification of dispersive clay soils. *Chin. J. Geotech. Eng.* **2005**, *27*, 75–81.
31. Wang, L.; Wang, D.M.; Bao, W.Z. Effect of Clay on Polycarboxylate Superplasticizer Performance and Mechanism Research. *J. Wuhan Univ. Technol.* **2013**, *35*, 6–9.
32. Yang, N.R. *Non-Tradition Cementitious Materials Chemistry*; Wuhan University of Technology Press: Wuhan, China, 2018; p. 179. (In Chinese)
33. Wang, P.M.; Xu, L.L.; Zhang, G.F. Formation and Conversion of Ettringite during Hydration of Portland Cement from 0 to 20 °C. *J. Chin. Ceram. Soc.* **2012**, *40*, 646–650. [CrossRef]
34. Gao, F.H.; Wang, L.; Liu, S.H. Deterioration Mechanism of Supersulfated Cement Paste by Acid Erosion. *Bull. Chin. Ceram. Soc.* **2022**, *41*, 2618–2627. [CrossRef]
35. Yang, N.R.; Yue, W.H. *The Handbook of Inorganic Metalloid Materials Atlas*; Wuhan University of Technology Press: Wuhan, China, 2000; pp. 277–278. (In Chinese)

Disclaimer/Publisher's Note: The statements, opinions and data contained in all publications are solely those of the individual author(s) and contributor(s) and not of MDPI and/or the editor(s). MDPI and/or the editor(s) disclaim responsibility for any injury to people or property resulting from any ideas, methods, instructions or products referred to in the content.